Ground Support 2026 - D Cumming-Potvin & J Wesseloo (eds.)
© 2026 Australian Centre for Geomechanics, Perth
doi:10.36487/ACG_repo/2625_03

Dynamic performance of ground support systems under impact loading tests: a deformation-based interpretation

Jorge Velásquez [a,*], Javier Vallejos [a,b], Ricardo Sepúlveda [a]

[a] *Advanced Mining Technology Center, University of Chile, Chile*

[b] *Department of Mining Engineering, University of Chile, Chile*

Abstract

This work presents an analysis of the dynamic response of ground support systems subjected to large-scale impact loading tests. The methodology integrates the estimation of the global dynamic demand from acceleration records, together with the evaluation of the local response of the reinforcement elements and the system displacement. The results show that support performance depends not only on the input energy, but also on the sequence of component activation and failure, load redistribution, and the degree of integration between mesh, shotcrete and anchorage elements. Three groups of field-scale tests are compared: stiff-impact tests on load-distribution systems (mesh-over-shotcrete configurations), stiff-impact tests on the central reinforcement element with high-tensile embedded mesh, and soft-impact tests incorporating an energy transfer bed. Across the families' groups, the mesh type and its installation (embedded versus over shotcrete), the bolt installation condition (grouted versus in a steel tube) and the presence of a load transfer bed are shown to govern the failure mode, the displacement at which the central element is eliminated and the post-failure energy absorption. This approach enables the comparison of different ground support systems in terms of their ability to control deformation, dissipate energy and maintain load transfer toward stable zones, while also providing a basis for the selection of design parameters under dynamic demand conditions.

Keywords: *dynamic testing, ground support systems, energy dissipation, load–displacement response, rockburst*

1 Introduction

Over recent decades, the exploitation of orebodies at greater depths has increased the exposure of underground excavations to high-stress environments, raising the occurrence of seismic events and rockbursts that represent a challenge for the safety and operational continuity of mines (Vallejos et al. 2024).

In this context, ground support systems constitute one of the main mechanisms for controlling instability of the rock mass. Their function is to maintain the integrity of the excavation and to protect personnel from the fall or ejection of rock associated with static and dynamic failure processes. In environments subjected to seismicity, support systems must maintain the stability of the excavation under the deformations generated by dynamic events, being capable of absorbing the released energy and preserving their containment capacity throughout the process (Li et al. 2014).

Modern support systems are composed of reinforcement elements, such as rockbolts and cable bolts, and of surface support elements, such as meshes and shotcrete. While the reinforcement elements contribute to stabilising the rock mass and absorbing load, the surface elements contain the fractured material and allow loads to be transferred to the anchorage elements (Vallejos et al. 2024). In this way, the global performance depends on the interaction between all its components and on their ability to act as an integrated system (Villaescusa et al. 2016).

[*] Corresponding author. Email address: jorge.velasquez@amtc.uchile.cl

For this reason, the assessment of support systems cannot be limited solely to the study of individual elements. Several authors have pointed out that the capacity of the complete system depends on the load transfer mechanisms, on the relative stiffness of its components and on the interaction between reinforcement and surface support (Potvin & Hadjigeorgiou 2015; Cuello et al. 2024). Consequently, the response observed in the field may differ significantly from that estimated based on the individual capacities of each component.

To improve the understanding of these mechanisms, over recent decades different dynamic tests have been developed to evaluate the behaviour of support systems under conditions representative of seismic events and rockbursts. Among them are the large-scale tests, which allow complete support configurations to be studied and parameters such as load, displacement, energy absorption and failure mechanisms to be analysed (Li et al. 2014).

In this context, the present work compares different configurations of support systems tested at large-scale, with the aim of analysing their behaviour through load, displacement, energy absorption and failure-mode parameters, identifying the main performance differences between the evaluated configurations. The tests are classified into 3 groups that share a common analysis methodology but differ in the impact regime and in the tested configuration: stiff-impact tests on load-distribution systems, in which the mesh type is isolated as the only variable; stiff-impact tests on the central reinforcement element with high-tensile embedded mesh; and soft-impact tests incorporating an energy transfer bed. This grouping allows the influence of the mesh type and its installation, of the bolt installation condition, and of the presence of a load transfer bed to be examined across a consistent framework.

2 Dynamic capacity of support systems: drop tests and large-scale tests

The exploitation of deeper orebodies has increased high-stress phenomena such as induced seismicity, strainbursts and rockbursts, requiring support systems capable of sustaining large displacements and dissipating energy beyond the scope of traditional static design; consequently, support design has evolved from strength- and equilibrium-based methodologies towards approaches centred on energy absorption and deformation capacity (Vallejos et al. 2024; Li et al. 2014). Performance under dynamic loading depends on the integrated response of the system rather than on its individual components; reinforcement elements (rockbolts and cable bolts) provide resistant capacity and energy absorption, while surface elements (meshes and shotcrete) contain the fractured rock mass and transfer load to the reinforcement. The system response is therefore governed by the interaction between components as damage progresses, and many failures result from a loss of load transfer capacity (Villaescusa et al. 2016; Cuello et al. 2024). This response has been investigated through component tests (Brändle et al. 2017), in situ blasting tests and large-scale free-fall impact tests conducted at specialised facilities such as the CANMET Mining and Mineral Sciences Laboratories (CANMET-MMSL, Canada), the Western Australian School of Mines (WASM, Australia), the Safety in Mines Research Advisory Committee facility (SIMRAC, South Africa) and the Geobrugg test site in Walenstadt (Switzerland), and is characterised through load, displacement, energy and failure-mode parameters, none of which should be interpreted in isolation, since the absorbed energy must be read together with the load–displacement response and the available capacity depends on the deformation history and the remaining capacity of each component (Kaiser & Moss 2022).

Differences in facilities, protocols and reported parameters hinder direct comparison between configurations (Potvin & Hadjigeorgiou 2015), so common analysis methodologies are required; central here is the impact regime defined by Vallejos et al. (2024), distinguishing stiff impacts, where the loading mass strikes the support directly, from soft impacts, where it first engages a load transfer bed representing the fractured surrounding rock – the gabion concept of Kaiser & Moss (2022). In soft impacts, much of the energy derived from accelerometer measurements is absorbed by the simulated rock rather than by the support; configurations must therefore be compared in terms of mechanism rather than absolute magnitude.

3 Interpreting large-scale impact tests through load, displacement and energy response

The dynamic tests are analysed following the Walenstadt large-scale impact methodology (Vallejos et al. 2024: Cuello et al. 2024). This approach distinguishes between the global dynamic demand applied to the support system, estimated from the accelerometer of the impacting block, and the local response measured at the instrumented anchors, considering the former the most representative and valid measurement of the dynamic demand applied to the system.

3.1 Physical model and reference frame

The analysed system corresponds to a rigid concrete block of mass m, released vertically from a defined height, which impacts the centre of the support system. The block is instrumented with a triaxial accelerometer, recording the acceleration in the vertical direction during the impact event.

A reference frame is adopted with the vertical axis z positive upwards. In the vertical direction, the block is subjected only to 2 forces: its self-weight W = mg, acting downwards, and the contact force exerted by the support system on the block, $F_c(t)$, acting upwards.

The contact force is estimated from the dynamic equilibrium of the block. Thus, the equation of motion of the block in the vertical direction is obtained from Newton's second law:

$$F_c(t) - mg = m \cdot \hat{a}_z(t) \quad (1)$$

where :

$\hat{a}_z(t)$ = the measured vertical acceleration of the block.

Solving for the contact force:

$$F_c(t) = m[\hat{a}_z(t) + g] \quad (2)$$

When the acceleration is expressed in dimensionless units of gravity, the equivalent global force can be written as:

$$F_c(t) = mg[1 + a_z(t)] \quad (3)$$

This force represents the global dynamic demand applied to the system.

3.2 Forces measured in the anchors

If the record of each load cell is denoted as $F_i(t)$, the total load of all the cells is described by the following equation:

$$F_{anchors}(t) = \Sigma F_i(t) \quad (4)$$

3.3 Estimation of displacement and energy

The global displacement of the system is obtained from the tracking of the block motion by means of high-speed cameras, allowing the estimated forces to be expressed as a function of the system displacement.

The energy transferred to the support system is calculated by integrating the load–displacement curve associated with the equivalent global force:

$$E_C(\delta) = \int_0^{\delta} F_c(\delta')\, d\delta' \quad (5)$$

Where:

$E_C(\delta)$ = the energy transferred to the support system up to a displacement δ

$F_c(\delta')$ = the equivalent global force (Equation 3) expressed as a function of displacement

δ = the global vertical displacement of the block

δ' = the integration variable for displacement.

Analogously, the energy associated with the response of the instrumented anchors is estimated by integrating the sum of forces measured at the anchors as a function of displacement:

$$E_{\Sigma}(\delta) = \int_0^{\delta} F_{\Sigma}(\delta')\, d\delta' \quad (6)$$

Where:

$E_{\Sigma}(\delta)$ = is the energy associated with the response of the instrumented anchors up to a displacement δ,

$F_{\Sigma}(\delta')$ = the total load measured at the anchors (Equation 4) expressed as a function of displacement.

3.4 Analysis procedure

In the analysis of the tests, several complementary analytical tools were constructed and used. Load–displacement and cumulative-energy–displacement graphs were produced from the global records of the block and from the sum of forces at the anchors, allowing both estimation methodologies to be compared. These records were correlated with the high-speed audiovisual material to chronologically identify the response mechanisms of the system, such as the onset of steel yielding, load redistribution, anchor rupture and mesh rupture. In addition, mechanical milestones were defined on the graphs by means of displacement and energy markers, which allowed the energy dissipated at each stage of the test to be quantified and the relative contribution of the different components of each system to be estimated.

4 Summary of test results

The dynamic response of 3 groups of ground support systems is presented and compared below, all analysed with the methodology of Section 3. The groups differ in the impact regime and in the tested support configuration (Figure 1):

1. stiff-impact tests on the load-distribution system (systems A and B), in which the mesh type is isolated as the only variable
2. stiff-impact tests on the central reinforcement element with high-tensile embedded mesh (group C, comprising the Test C1, Test C2 and Test C3)
3. soft-impact tests incorporating an energy transfer bed (systems E and F).

Following the classification of Vallejos et al. (2024), systems A to C are stiff-impact tests, in which the loading mass impacts the support directly, whereas systems E and F are soft-impact tests, in which the loading mass first impacts the energy transfer bed. Consistent with the gabion concept introduced by Kaiser & Moss (2022), the transfer bed represents the fractured rock surrounding an in situ excavation rather than a component of the support system itself. As a reference for interpreting the system response, Figure 2 presents the load–displacement curves of the individual support elements (bolts, cables and meshes) used in the test programme, as reported in previous laboratory tests.

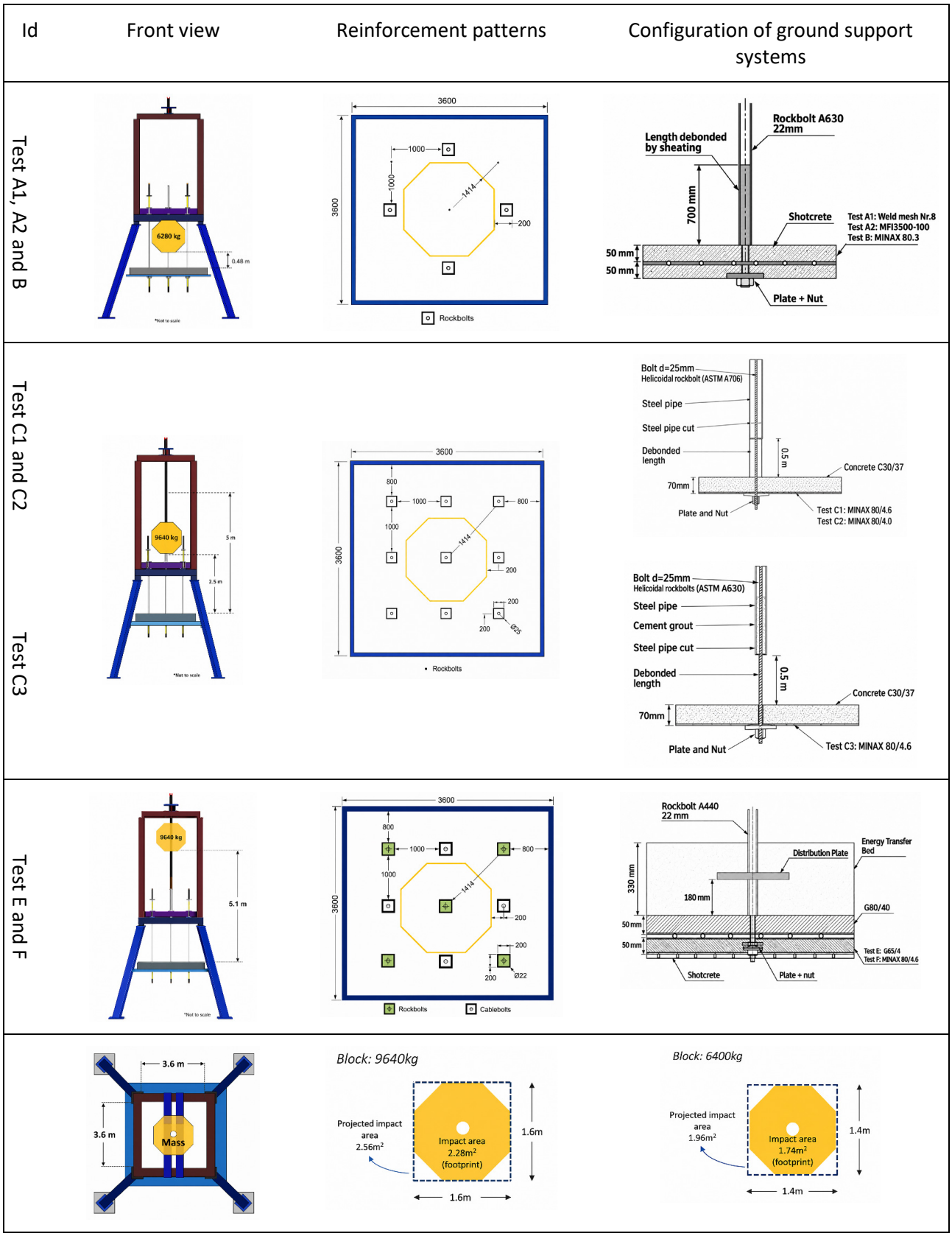


Figure 1 **Test arrangement, reinforcement patterns and configuration of ground support systems for ground support A, B, C, E, and F, respectively. Plan scheme of testing apparatus and plan view of loading blocks (modify from Vallejos et al. [2024])**

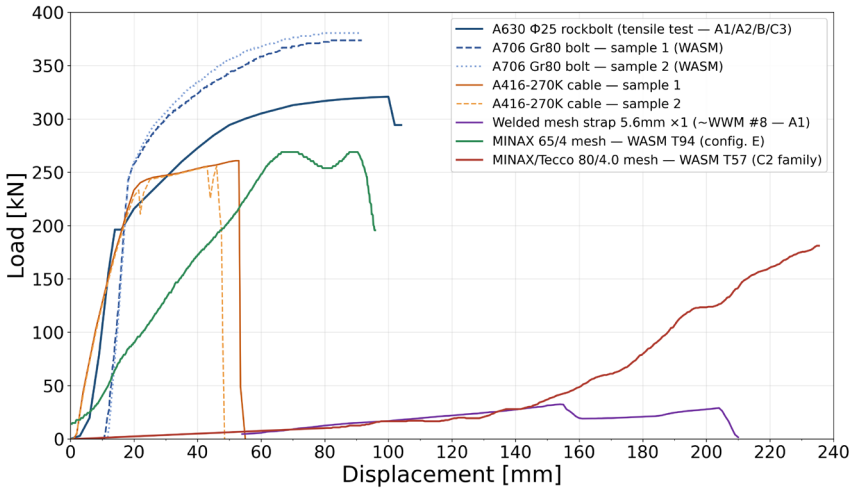


Figure 2 Load–displacement curves of individual ground support elements (bolts, cables and meshes) present in the dynamic test programme (Player et al. 2008; Vallejos et al. 2022)

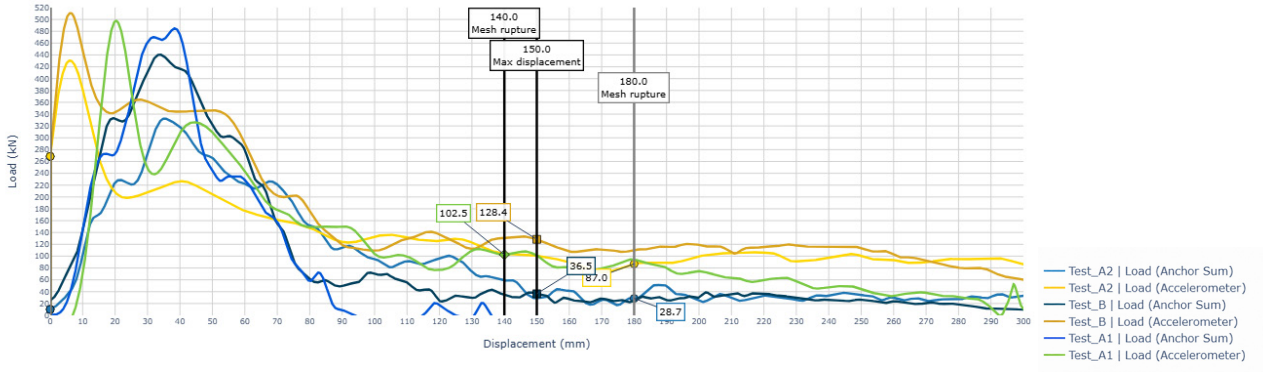
4.1 Surface support system under stiff impact (systems A and B)

The first group isolates the influence of the mesh type. Systems A and B were nominally identical – loading mass of 6,280 kg, drop height of 0.48 m, nominal input energy of 30 kJ, four 22 mm A630 rockbolts grouted in a steel tube with a 0.70 m debonded length, and 100 mm of fibre-reinforced shotcrete – and differed only in the mesh embedded in the shotcrete: a conventional welded wire mesh (AWG#8, 3.26 mm wire) in Test A1, an MFI3500-100 mesh in Test A2 and a high-tensile chain-link mesh (MINAX 80/3, 3 mm wire) in Test B. This makes the group a cleaner comparison of the mesh than the remaining tests, in which the drop height, the steel grade or the bolt installation condition co-vary. Table 1 summarises the configuration and the main results.

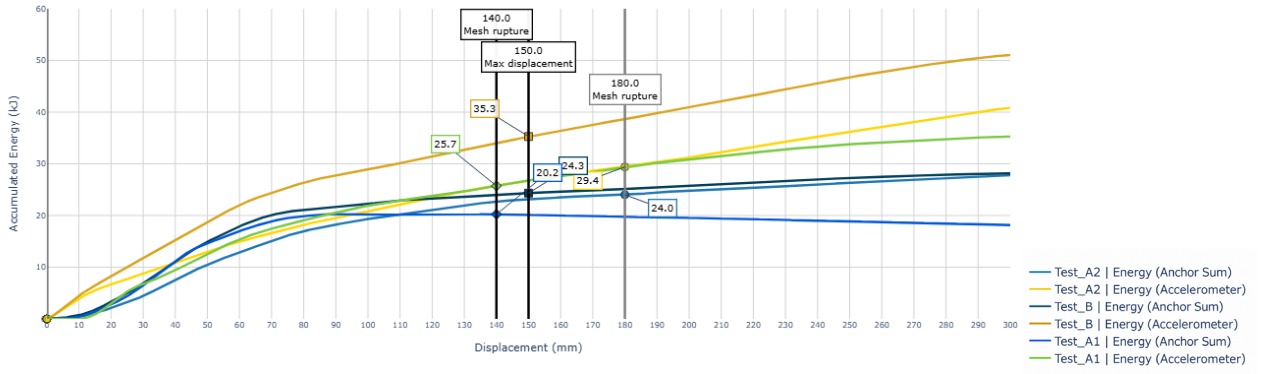
Table 1 Configuration and main results of the stiff-impact tests on load-distribution systems (systems A and B)

Parameter	Test A1 (WWM #8)	Test A2 (MFI3500)	Test B (MINAX 80/3)
Mesh type	Welded mesh #8	MFI3500-100	MINAX 80/3
Bolt total length (m)	2.4	2.4	2.4
Bolt debonded length from the collar (m)	0.70	0.70	0.70
Bolt bonded length (m)	1.7	1.7	1.7
Nominal input energy (kJ)	30	30	30
Maximum measured energy (kJ)	25.7	29.4	35.3
Displacement at mesh rupture (mm)	140	180	No global rupture
Maximum deflection (mm)	–	–	150
Rupture time (ms)	≈ 80	≈ 83	–
Block retained	No	No	Yes

The load–displacement and cumulative-energy responses of the 3 configurations are shown in Figure 3. The most relevant result was qualitative: under the same 30 kJ input energy, the 2 conventional meshes failed by rupture without retaining the block, whereas the high-tensile mesh retained the block without global rupture. The welded wire mesh (Test A1) ruptured at approximately 140 mm, with a deformation energy of 25.7 kJ, and the MFI3500-100 mesh (Test A2) ruptured at approximately 180 mm, with 29.4 kJ. In contrast, the MINAX 80/3 mesh showed no global rupture and retained the block, reaching a maximum energy of the order of 35.3 kJ at a maximum deflection close to 150 mm. Thus, while the conventional meshes failed at or below the input energy, the high-tensile mesh absorbed an energy above the input without losing its global integrity.



(a)



(b)

Figure 3 Response of the load-distribution systems tested under stiff impact (Tests A1, A2 and B), from accelerometer and anchor-sum records: (a) load versus displacement; (b) cumulative energy versus displacement. Vertical lines mark mesh rupture in Test A1 (140 mm) and Test A2 (180 mm), and the maximum displacement reached in Test B (150 mm)

From Figure 3, the results demonstrate that, keeping all the other components of the system constant and under the same demand, the mesh type alone determines the transition between retention and collapse of the block. The high-tensile MINAX 80/3 mesh provided the combination of load capacity and deformation capacity required to contain the impacting mass, whereas the conventional meshes exhausted their capacity by rupture before dissipating the whole input energy. Because the gap between accelerometer and anchor-sum records is much narrower in this stiff-impact family than in the soft-impact tests, the absence of a gabion means that the demand is transmitted almost directly to the instrumented reinforcement, so the comparison isolates the mesh contribution particularly well. It is also noted, following Vallejos et al. (2024), that the perpendicular cut in the steel tube (split-tube) introduces a strain localisation that renders the reinforcement elements more ductile in the tests, so part of the recorded deformation capacity stems from the experimental arrangement rather than solely from the intrinsic response of the system. Across this group, no bolt failure or slippage through the grout was reported: the block was lost through mesh rupture rather

than through the reinforcement, with maximum recorded anchor forces of 173 kN in Test A1 and approximately 94 kN in Test A2.

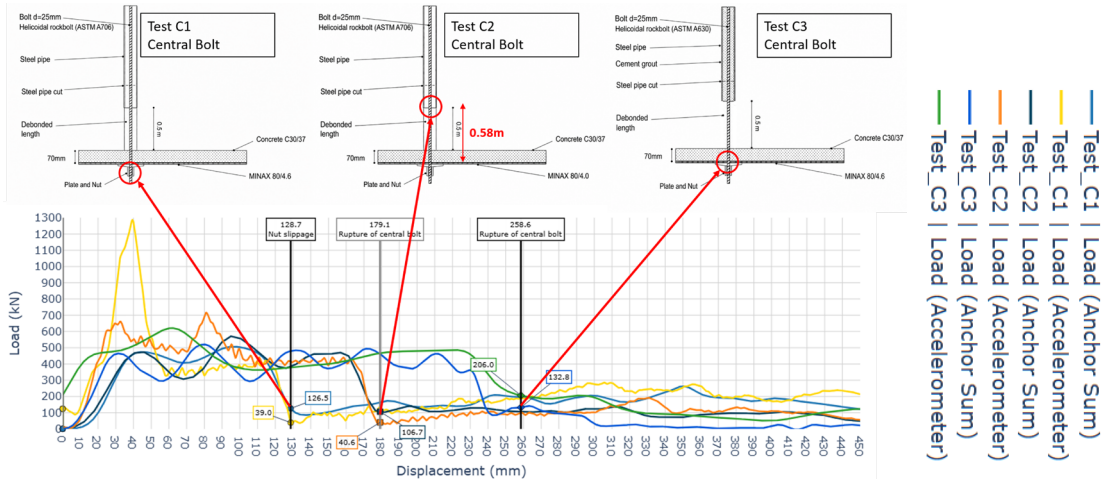
4.2 Reinforcement systems under stiff impact with high-tensile embedded mesh (group C)

The second group corresponds to stiff-impact tests in which the loading mass impacts the central reinforcement element directly, over a high-tensile chain-link mesh and 70 mm of shotcrete. Three tests share this configuration base: Test C1 (MINAX 80/4.6 mesh, A706 G80 bolts in a steel tube), Test C2 (MINAX 80/4.0 mesh, A706 G80 bolts in a steel tube) and Test C3 (MINAX 80/4.6 mesh, A630 bolts fully grouted). The main differences between the 3 tests are therefore the mesh type, the bolt steel grade and, most decisively, the bolt installation condition. Table 2 summarises the configuration and the key results.

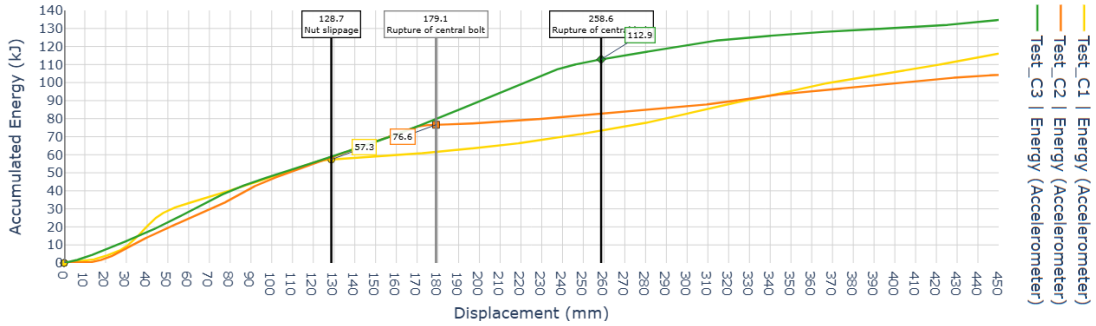
Table 2 Configuration and main results of the stiff-impact tests on reinforcement systems with high-tensile mesh (group C)

Parameter	Test C1	Test C2	Test C3
Mesh	MINAX 80/4.6	MINAX 80/4.0	MINAX 80/4.6
Bolt steel grade	A706 G80	A706 G80	A630
Bolt installation	Steel tube (no grout)	Steel tube (no grout)	Fully grouted
Installation procedure	Decoupled Ø25 mm bolt installed inside a steel tube (split-tube, no grout); load transferred only through plate and nut	Decoupled Ø25 mm bolt installed inside a steel tube (split-tube, no grout); load transferred only through plate and nut	Ø25 mm bolt fully cement-grouted along its length
Debonded (free) length (m)	0.5	0.5	0.5
Nominal input energy (kJ)	229.8	229.8	236.2
Central-bolt failure	Nut slippage	Bolt shear	Bolt shear
Displacement at bolt failure (mm)	128.7	179.1	258.6
Accumulated energy at bolt failure (kJ)	57.3	76.6	112.9
Displacement at mesh collapse (mm)	359.9	345.1	–

Figure 4 presents the individual load–displacement and cumulative-energy responses of the 3 tests. In Test C1, 3 main milestones were identified: shotcrete rupture, nut slippage at the central bolt at 128.7 mm and mesh collapse at 359.9 mm. At the instant of nut slippage, the accumulated energy estimated by the accelerometer was 57.3 kJ, against 44.6 kJ recorded by the anchor sum; at collapse, the energy reached approximately 97.9 and 83.5 kJ, respectively. From the onset of slippage to final collapse, both estimates showed a convergent trend in load and in accumulated energy, indicating that the response became controlled by the joint interaction of mesh, bolts and remaining shotcrete elements, and that the observed behaviour cannot be attributed to the MINAX mesh alone but to the integrated performance of the mesh–anchor–shotcrete assembly.



(a)



(b)

Figure 4 Response of the group C tests (Tests C1, C2 and C3) with the central-bolt failure mode: (a) load versus displacement from accelerometer and anchor-sum records, with schematics of the central-bolt installation condition and the location of failure in each test (red circles); (b) cumulative energy versus displacement from accelerometer records. Vertical lines mark nut slippage in Test C1 (128.7 mm) and rupture of the central bolt in Tests C2 (179.1 mm) and C3 (258.6 mm)

In Test C2, 3 main milestones were identified: shotcrete rupture at 20.4 mm, central-bolt shear at 179.1 mm and mesh collapse at 345.1 mm. At the instant of bolt shear, the recorded load was 106.7 kN by the anchor sum and 40.6 kN by the accelerometer, with accumulated energies of 64.6 and 76.6 kJ; at collapse, the loads were 70.2 and 97.7 kN, with accumulated energies of 83.3 and 93.5 kJ. After bolt shear, both load curves exhibited a comparable response, evidencing the redistribution of stresses and the transfer of load towards the remaining elements of the system, presumably the mesh and the shotcrete fragments still active by interlocking.

4.2.1 Joint comparison: the central-bolt failure mechanism

When the 3 tests are analysed together (Figure 4), the displacement at which the central bolt is lost defines a marked progression: 128.7 mm in Test C1, 179.1 mm in Test C2 and 258.6 mm in Test C3. This progression of +50.4 and +79.5 mm between successive tests is accompanied by an equal increase in the accelerometer-derived accumulated energy at the instant of bolt failure: 57.3, 76.6 and 119.1 kJ, respectively. Test C3 not only delayed the central-bolt failure by 79.5 mm relative to Test C2, but also accumulated about 36.3 kJ of additional energy before that event.

The failure mode differs systematically along the series and allows this progression to be interpreted. In Test C1, the loss of capacity of the central bolt occurred by nut slippage, a mechanism of progressive loss of resistant capacity that manifested early. In Test C2, the central bolt failed by shear – a more abrupt failure of the element – at a larger displacement, apparently in the contact zone between the bar and the steel tube; this condition may have allowed a local rotation or stress concentration that favoured a premature shear

mechanism. In Test C3, with bolts fully grouted along their length and without a split-tube, the bolt shear shifted further and occurred at the plate–nut contact. The joint comparison suggests that the bolt installation condition dominantly governs the displacement and energy at which the central support element is lost; the absence of grout and the presence of the tube (Test C1 and C2) favour localised, premature failure mechanisms, whereas full grouting (Test C3) restricts the lateral movement and rotation of the bolt, forcing the demand to concentrate at the plate–nut–washer contact and deferring the failure towards larger displacements and energies.

It should be emphasised, however, that these comparisons do not isolate a single variable. Test C3 used a slightly larger mass and therefore a higher impact energy (236.2 against 229.8 kJ for the C1, and C2 Tests), which probably contributed to the bolt shear and the mesh collapse occurring within a narrower displacement interval; in addition, Test C3 used A630 bolts instead of A706 G80. Since in Test C2 the bolt failed in the contact zone with the tube, the observed response does not necessarily represent the real capacity of the A706 steel within the system, as the mechanism may have been governed by the bar–tube interaction rather than by the resistant exhaustion of the material. Consequently, it is not possible to conclusively attribute the improved performance of Test C3 to a single factor – mesh, steel grade or grouting condition – even though the body of evidence points to the grouted installation condition as the factor of greatest influence on the deferral of the central-bolt failure.

4.2.2 Post-failure behaviour and the role of the mesh

A second axis of comparison emerges when examining the response after bolt failure, where the order of performance is reversed with respect to the failure displacement. Between the C1 and C2 tests, which share steel grade and installation condition and differ only in the mesh, Test C1 (MINAX 80/4.6) accumulated an additional post-failure absorption of the order of 40.6 kJ between nut slippage (57.3 kJ at 128.7 mm) and mesh collapse (97.9 kJ at 359.9 mm), whereas Test C2 (MINAX 80/4.0) accumulated only about 16.9 kJ between bolt shear (76.6 kJ at 179.1 mm) and collapse (93.5 kJ at 345.1 mm). Thus, although Test C2 developed a greater capacity prior to the central-bolt failure, test C1 exhibited a considerably more robust post-failure response, attributable to a greater load-redistribution capacity of the MINAX 80/4.6 mesh and to a more effective mechanical interaction between mesh, shotcrete and remaining support elements. In all 3 tests, the recorded energy corresponds to the global performance of the complete system – mesh, bolts and shotcrete – and not to the individual behaviour of any of its components.

4.3 Support systems under soft impact with an energy transfer bed (systems E and F)

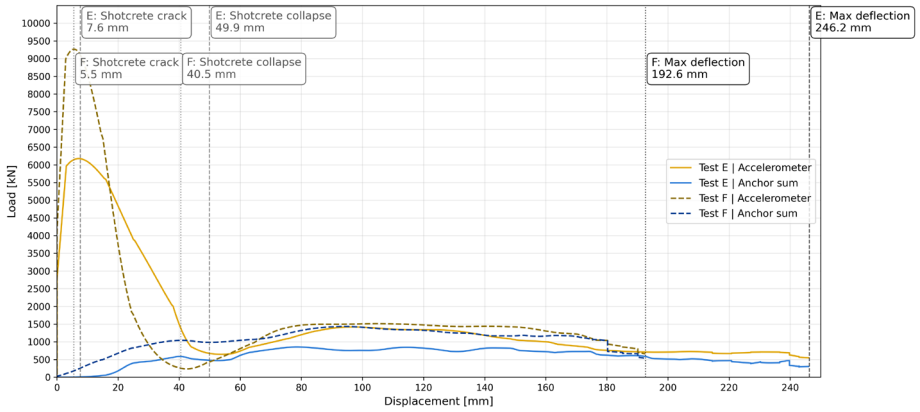
The third group corresponds to soft-impact tests, in which the loading mass first impacts a 330 mm energy transfer bed before engaging the support system. As noted above, this bed does not form part of the support system: it represents the fractured rock around an in situ excavation and acts under the gabion concept of Kaiser & Moss (2022). This distinction is decisive for the interpretation, because the accelerometer curve measures the global demand including the energy absorbed by the simulated rock, whereas the anchor sum measures only the load that reaches the reinforcement elements. Both configurations were nominally identical – block mass of approximately 9,600 kg, 2 mesh layers, 5 active A440 rockbolts, 4 twin cable bolts, 100 mm shotcrete and a 330 mm transfer bed – and differed in 2 parameters: the drop height (5.05 m for E, 4.9 m for F) and the external mesh (MINAX 65/4 for E, MINAX 80/4.6 for F). The corresponding input energies were 476 and 461 kJ. Table 3 summarises the configuration and the main results.

The load–displacement and cumulative-energy responses of Test E and F are shown in Figure 5. Both systems retained the block without final failure, which is the first-order performance result. At the collapse of the shotcrete, the accelerometer-derived accumulated energy reached 258.3 kJ at 49.9 mm in Test E and 290.0 kJ at 40.5 mm in Test F; Test F thus accumulated 31.7 kJ more energy while doing so at a smaller displacement. At maximum system deflection, the accelerometer curves approached the nominal input energies of each test, while the anchor-sum curves reached approximately 145 kJ in both cases. The resulting gap between the 2 estimates was comparable across tests (of the order of 305 kJ in E and 315 kJ in F), with the instrumented anchors accounting for roughly 31–32% of the total energy registered by the accelerometer in both

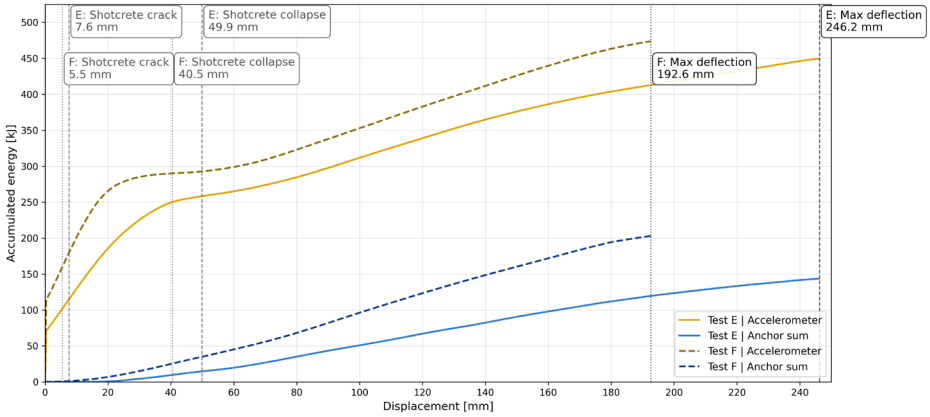
configurations. This indicates that, in both soft-impact tests, the majority of the input energy was dissipated outside the instrumented reinforcement elements – that is, within the mesh, the shotcrete and the transfer bed.

Table 3 Configuration and main results of the soft-impact tests with an energy transfer bed (systems E and F)

Parameter	Test E	Test F	Parameter
External mesh	MINAX 65/4	MINAX 80/4.6	External mesh
Drop height (m)	5.05	4.9	Drop height (m)
Input energy (kJ)	476	461	Input energy (kJ)
Accumulated energy at shotcrete collapse (kJ)	258.3 (at 49.9 mm)	290.0 (at 40.5 mm)	Accumulated energy at shotcrete collapse (kJ)
Accelerometer energy, final (kJ)	≈ 450	≈ 474	Accelerometer energy, final (kJ)
Anchor-sum energy, final (kJ)	≈ 143	≈ 203	Anchor-sum energy, final (kJ)
Maximum deflection (mm)	246.2	192.6	Maximum deflection (mm)
Energy per unit displacement (kJ/mm)	1.93	2.39	Energy per unit displacement (kJ/mm)
First damage	Yield bolt	Cable damage	First damage
Block retained	Yes	Yes	Block retained



(a)



(b)

Figure 5 Response of support systems E (MINAX 65/4 external mesh) and F (MINAX 80/4.6 external mesh) under soft impact: (a) load versus displacement; (b) cumulative energy versus displacement. Solid lines correspond to Test E and dashed lines to Test F. Blue curves are from the anchor sum and yellow curves are from the accelerometer-derived equivalent load. Vertical lines mark shotcrete cracking, shotcrete collapse and maximum deflection in each test

To place this result in the context of the whole test series, Figure 6 compares the absorbed energy and the remaining capacity of all tested configurations, normalised by the energy absorbed at 100 mm (E_{100}); these curves are discussed in Section 4.3.3.

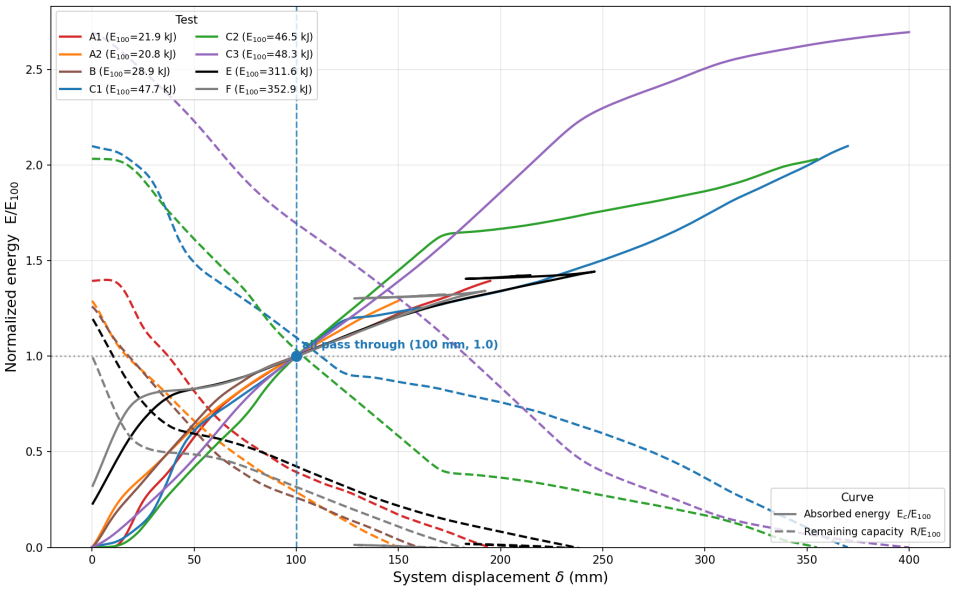


Figure 6 Normalised absorbed energy (E/E_{100}, solid lines) and remaining capacity (R/E_{100}, dashed lines) versus system displacement for all tested configurations (Tests A1, A2, B, C1, C2, C3, E and F). Curves are normalised by the energy absorbed at 100 mm (E_{100}), so that all of them pass through (100 mm, 1.0)

4.3.1 Load transfer and curve coupling

A marked difference between the 2 tests was observed in the relationship between the 2 load estimates. In Test E, the accelerometer curve remained consistently above the anchor-sum curve throughout the post-collapse response, the 2 estimates remaining decoupled. In Test F, the 2 load curves converged after the collapse of the shotcrete, tracking one another closely from approximately 130 mm onward. The convergence of the load curves in Test F suggests that the higher-tensile external mesh (MINAX 80/4.6) promoted a more direct transfer of the global demand toward the instrumented reinforcement, whereas the lower-capacity mesh of Test E (MINAX 65/4) distributed the load more diffusely between the mesh, the shotcrete and the transfer bed, sustaining the decoupling. This interpretation is consistent with the earlier engagement of the cable bolts inferred from the first-damage sequence – cable damage in F versus bolt yielding in E – and with the higher absorption density and smaller deflection recorded in Test F. It should nonetheless be noted that the curve convergence in Test F constitutes stronger evidence of a genuine transfer mechanism than the divergence in Test E does of a specific one: part of the gap in Test E may reflect instrumentation limitations, given that only 5 of 9 bolts were active and that load may have travelled through uninstrumented paths.

4.3.2 Displacement response

The maximum system deflection was 246.2 mm in Test E and 192.6 mm in Test F, a difference of 53.6 mm (27.8%). Expressed as input energy per unit of maximum displacement, Test F absorbed 2.39 kJ/mm against 1.93 kJ/mm for Test E, corresponding to a 1.24-fold higher absorption density. Although Test E received only 3.3% more input energy than Test F, its maximum deflection exceeded that of Test F by 27.8%, a difference disproportionate to the input energy alone. This behaviour is consistent with the curve coupling described above: when the bolts and cables take up load earlier and more directly, as in Test F, the total deformation of the system is limited. Because the 2 tests differed simultaneously in drop height and external mesh, the effect of the mesh cannot be isolated from that of the input energy, and the comparison should be regarded

as interpretive rather than conclusive. Furthermore, since a substantial fraction of the accelerometer-registered energy is dissipated within the transfer bed – which represents the surrounding rock rather than the support – a component-wise decomposition of the dissipated energy, separating the contribution of the gabion from that of the support system, is required before the energy performance of the 2 mesh configurations can be compared on a common basis.

4.3.3 Remaining-capacity curves

Following the deformation-based support design (DBSD) framework of Kaiser & Moss (2022), the records were reinterpreted as remaining-capacity curves, in which the mobilisable capacity is the complement of the absorbed energy with respect to the total energy of the test. Figure 6 presents these curves normalised by E100, the energy absorbed at 100 mm, defined as a design parameter for reinforcement selection by Cai & Kaiser (2018), which anchors every configuration at a common physical displacement while preserving the real deformation scale. In all 8 configurations the remaining capacity starts at its installed value and decays monotonically to zero at collapse, confirming experimentally the central DBSD principle that capacity is consumed with displacement, so the relevant capacity for design is the one remaining at the instant of loading rather than the installed one. The normalisation further separates the groups by the rate at which that capacity is consumed: groups C sustains a pronounced slope beyond the reference and extends to 2.5–4 times the 100 mm reference, evidencing continued mobilisation and a larger deformation reserve, whereas the soft-impact systems (E/F) absorb most of the demand before 100 mm — their high apparent E100 (~312–353 kJ) overstating the capacity attributable to the support, because the transfer bed absorbs much of the early demand. These readings support the conclusion that system robustness is best expressed as the deferral of the exhaustion of the remaining capacity rather than the maximisation of nominal energy.

5 Conclusion

The dynamic response of 3 groups of ground support systems was analysed under a common load–displacement–energy framework, distinguishing the global demand estimated from the block accelerometer from the local response measured at the instrumented anchors. Across the 3 groups, support performance was shown to depend not only on the input energy but on the sequence of component activation and failure, on load redistribution and on the degree of integration between mesh, shotcrete and anchorage.

In the stiff-impact tests on load-distribution systems (systems A and B), where the mesh was the only variable, the mesh type alone determined the transition between retention and collapse of the block: under the same 30 kJ input energy, the conventional welded wire and MFI3500 meshes ruptured without retaining the block, whereas the high-tensile MINAX 80/3 mesh retained it without global rupture. This is the clearest isolated effect of the mesh in the whole series.

In the stiff-impact tests on reinforcement systems with high-tensile embedded mesh (group C), the displacement at which the central bolt was lost followed a monotonic progression – 128.7, 179.1 and 258.6 mm for Tests C1, C2 and C3 – accompanied by a monotonic increase in accumulated energy at failure. The evidence points to the bolt installation condition (grouted versus in a steel tube) as the dominant factor governing the deferral of the central-bolt failure, although the mass, steel grade and mesh co-vary and prevent a single-variable attribution. In the post-failure stage, the order reverses: the MINAX 80/4.6 configuration (Test C1) absorbed markedly more energy after failure than the MINAX 80/4.0 configuration (Test C2), indicating a greater residual load-redistribution capacity.

In the soft-impact tests with an energy transfer bed (Test E and F), both systems retained the block without final failure. The energy gap between the accelerometer and the anchor sum was comparable in both tests (≈ 68–69% of the energy dissipated outside the instrumented reinforcement), confirming that in a soft-impact test a large part of the dissipation occurs in the mesh, the shotcrete and the gabion, and should not be attributed in full to the support. System F, with the higher-tensile external mesh, showed converging load curves and a higher absorption density (2.39 versus 1.93 kJ/mm), retaining a block of comparable energy in 54 mm less displacement – a stiffer, more efficient response.

Reinterpreting the records as remaining-capacity curves under the DBSD framework of Kaiser & Moss (2022), normalised by the energy absorbed at 100 mm (E100), confirmed that support capacity is consumed with displacement and decays to zero at collapse, so the capacity relevant for design is the one remaining at the instant of loading, not the installed one. The normalisation also separated the groups by the rate of consumption: group C sustained capacity well beyond the reference, evidencing a larger deformation reserve, whereas the soft-impact systems consumed most of their capacity before 100 mm, their high apparent E100 overstating the support contribution because the transfer bed absorbs much of the early demand. System robustness is thus better expressed as the deferral of capacity exhaustion than as the maximisation of nominal energy.

Acknowledgement

The authors wish to express their sincere gratitude to the Advanced Mining Technology Centre, Universidad de Chile for financially supporting this study with the baseline project ANID CIA250010.

References

Brändle, R, Rorem, E, Luis, R & Fischer, G 2017, 'Full-scale dynamic tests of a ground support system using high-tensile strength chain-link mesh in El Teniente mine, Chile', in M Hudyma & Y Potvin (eds), *UMT 2017: Proceedings of the First International Conference on Underground Mining Technology*, Australian Centre for Geomechanics, Perth, pp. 25–43, https://doi.org/10.36487/ACG_rep/1710_01_Luis

Cai, M & Kaiser, PK 2018, *Rockburst Support Reference Book, Volume I: Rockburst Phenomenon and Support Characteristics*, MIRARCO – Mining Innovation Rehabilitation and Applied Research Corporation, Laurentian University, Sudbury.

Cuello, D, Orrego, C, Vallejos, J & Velásquez, J 2024, 'The role of surface support in controlling rockbursting conditions', in D Johansson & H Schunnesson (eds), *MassMin 2024: Proceedings of the 9th International Conference & Exhibition on Mass Mining*, Luleå University of Technology, Luleå, pp. 948-964, https://doi.org/10.36487/ACG_repo/2435_G-07

Kaiser, PK & Moss, A 2022, 'Deformation-based support design for highly stressed ground with a focus on rockburst damage mitigation', *Journal of Rock Mechanics and Geotechnical Engineering*, vol. 14, pp. 50–66.

Li, CC 2014, 'Principles of rockbolting design', *Journal of Rock Mechanics and Geotechnical Engineering*, vol. 6, no. 2, pp. 105–116.

Player, JR, Morton, EC, Thompson, AG & Villaescusa, E 2008, 'Static and dynamic testing of steel wire mesh for mining applications of rock surface support', *Proceedings of the Sixth International Symposium on Ground Support in Mining and Civil Engineering Construction*, The Southern African Institute of Mining and Metallurgy, Cape Town, pp. 693–706.

Potvin, Y & Hadjigeorgiou, J 2015, 'Empirical ground support design of mine drives', in Y Potvin (ed.), *Design Methods 2015: Proceedings of the International Seminar on Design Methods in Underground Mining*, Australian Centre for Geomechanics, Perth, pp. 419-430, https://doi.org/10.36487/ACG_rep/1511_25_Potvin

Vallejos, JA, Bucher, R & Álvarez, R 2022, 'Analysis of the behavior of the weld mesh and the rolled mesh against static loads and a dynamic impact, to design the overlap according with the connection method', *Proceedings of the 10th International Symposium on Rockbursts and Seismicity in Mines (RaSiM10)*, Society for Mining, Metallurgy & Exploration, Englewood.

Vallejos, JA, Marambio, E, Burgos, L, Cuello, D, Brändle, R, Luis, R, von Rickenbach, G & Fischer, G 2024, 'Dynamic test response of ground support systems for underground excavations at the Walenstadt testing facility', *Rock Mechanics and Rock Engineering*, vol. 57, pp. 389–428, https://doi.org/10.1007/s00603-023-03547-1

Villaescusa, E, Thompson, AG & Player, JR 2016, 'Dynamic testing of combined rock bolt and mesh schemes', in *Proceedings of the Seventh International Conference and Exhibition on Mass Mining (MassMin 2016)*, The Australasian Institute of Mining and Metallurgy, Melbourne.